

## ARTICLE

DOI: 10.1038/s42005-018-0081-9

OPEN

# Breakdown of diffusivity–entropy scaling in colloidal glass-forming liquids

Bo Li<sup>1,2,3</sup>, Xiuming Xiao<sup>1</sup>, Kai Lou<sup>1,3</sup>, Shuxia Wang<sup>1</sup>, Weijia Wen<sup>1,2</sup> & Ziren Wang<sup>1</sup>

Glass is a liquid that has lost its ability to flow. Why this particular substance undergoes such a dramatic kinetic slowdown yet remains barely distinguishable in structure from its fluid state upon cooling constitutes the central question of glass transition physics. Here, we investigate the pathway of kinetic slowdown in glass-forming liquids that consist of monolayers of ellipsoidal or binary spherical colloids. In contrast to rotational motion, the dynamics of the translational motion begin to violently slow down at considerably low area fractions ( $\phi_T$ ). At  $\phi_T$ , anomalous translation–rotation coupling is enhanced and the topography of the free energy landscape become rugged. Based on the positive correlation between  $\phi_T$  and fragility, the measurement of  $\phi_T$  offers a novel method for predicting glassy dynamics, circumventing the prohibitive increase in equilibrium times required in high-density regions. Our results highlight the role that thermodynamical entropy plays in glass transitions.

<sup>1</sup>Key Laboratory of Soft Condensed Matter Physics and Smart Materials, College of Physics, Chongqing University, Chongqing 401331, China. <sup>2</sup>Department of Physics, Hong Kong University of Science and Technology, Clear Water Bay, Hong Kong 999077, China. <sup>3</sup>Center for Soft and Living Matter, Institute of Basic Science, Ulsan 44919, South Korea. Correspondence and requests for materials should be addressed to B.L. (email: [libotc@gmail.com](mailto:libotc@gmail.com)) or to Z.W. (email: [wziren@cqu.edu.cn](mailto:wziren@cqu.edu.cn))

As a prevalent state of matter, glasses are ubiquitous in nature. Various types of glass are manufactured at industrial scales and possess particularly desirable mechanical or optical properties that are useful in a wide variety of applications in daily life. However, achieving a consistent microscopic understanding of the behaviours of glass remains a challenge for both physicists and material scientists<sup>1</sup>. One central problem in glass science is kinetic slowdown, which is the process through which a liquid loses its ability to flow upon cooling. Why this particular substance undergoes such dramatic slowdown kinetically but does not appear to undergo structural changes during the glass transition has been extensively investigated<sup>2</sup>.

The theories of random first order transition<sup>3</sup> and dynamical facilitation<sup>4</sup> have achieved great success in the study of glass transitions. For example, the heterogeneous dynamics and structures predicted by these theories have been repeatedly confirmed in both experiments<sup>5–8</sup> and simulations<sup>9–11</sup>. In an alternative approach, the process of kinetic slowdown was determined to be directly related to the thermodynamical quantities of enthalpy and entropy<sup>12</sup>, which were eventually determined by the topography of the free energy landscape (FEL)<sup>13</sup>; however, experimental tests of FEL in glassy systems have been rare<sup>14</sup>.

Despite an abundance of theories, however, knowledge gaps remain and preclude a thorough understanding of glassy dynamics which hinders a broader application of them. One interesting research topic is translation–rotation coupling in molecular liquid and how such a coupling influences glassy behaviours. It was predicted by mode coupling theory (MCT) that the sequence of glass transitions in translational and rotational degrees of freedom depended on the shape factor of the non-spherical motif<sup>15,16</sup>. However, how the collision of neighbouring non-spherical motifs within a small distance influences glassy dynamics involving collective motion on a much larger length scale has remained poorly understood. Also, experiments have yet to establish a clear link between kinetics and thermodynamics in glass transition<sup>17</sup>.

Excess entropy ( $s^{ex}$ ), which is a measure of inherent structures within a basin<sup>13</sup>, has been served as an excellent descriptor of the FEL topography, and therefore has been used to describe the kinetic slowdown of glass-forming liquids<sup>18</sup>. Additionally, the frequency of collisions, which defines the rate at which the system relaxes, is proportional to the number of accessible configurations<sup>19,20</sup>. This argument directly leads to a scaling law between the long-time diffusion constant and excess entropy ( $D-s^{ex}$  scaling) as  $D \sim e^{-\alpha s^{ex}}$ . Although the  $D-s^{ex}$  scaling for rotational degree of freedom (superscript ‘ $\theta$ ’) has remained unexplored, the  $D \sim e^{-\alpha s^{ex}}$  relation in the translational degree of freedom (superscript ‘ $T$ ’ in this paper) has been verified in atomic<sup>21</sup>, granular<sup>22</sup> and colloidal liquids<sup>23–25</sup>. More critically, this exponential scaling ( $D \sim e^{-\alpha s^{ex}}$ )<sup>19,26</sup> has been proverbially used as a tool for discovering liquid properties such as the anomalous behaviours of water<sup>27–29</sup>, atom diffusivity in porous materials<sup>30</sup>, the confinement effect in fluids<sup>31</sup>, and the relaxation of glass-forming liquids<sup>32</sup> and quasicrystals<sup>19</sup>; it has become a standard feature of a liquid. However, this  $D-s^{ex}$  scaling has only been verified for liquids at packing fractions considerably higher than the melting point ( $\phi_m$ ) or glass transition point ( $\phi_g$ ). The term  $\phi$  is equivalent to the inverse of temperature in a molecular system—higher  $\phi$  in colloids means a lower effective temperature. When approaching  $\phi_g$ , a glass-forming liquid becomes dense and dynamically heterogeneous<sup>33</sup>. Theoretically, the  $D^T-s^T$  scaling takes a more precipitous form as  $D \sim e^{\frac{\alpha}{T} s^{ex}}$  near  $\phi_g$ <sup>12</sup>, where the superscript ‘ $T$ ’ represents the translational degree of freedom. Consequently, it is reasonable to expect the  $D-s^{ex}$  scaling to break down at some point upon cooling, at least for

glass-forming liquids. Because the  $D-s^{ex}$  scaling is a joint product of thermodynamical entropy and the dynamic diffusion coefficient, it can be usefully employed to study the role that thermodynamics plays in the kinetic slowdown during glass transitions<sup>18</sup>.

Colloids have served as an outstanding model for investigating glass transitions<sup>34</sup>. Micro-particles dispersed in water undergo Brownian motion, which perfectly simulates the diffusion of atoms or molecules<sup>35</sup>. The motion of each particle can be recorded and digitalised using optical video microscopy<sup>36</sup>. Consequently, kinetic information with single-particle resolution can always be obtained using these platforms. The typical relaxation time of a colloidal glass is seconds to hours depending on  $\phi$ <sup>6</sup>, which makes the systematic testing of glassy dynamics possible. Numerous theoretical models of glass transitions have been evaluated in colloidal systems, namely dynamical heterogeneity (DH)<sup>5–7</sup>, the point-to-set approach<sup>37</sup> and dynamical facilitation<sup>38</sup>.

In this study, we systematically investigated the kinetic slowdown of two crystallising and eight glass-forming liquids by measuring their  $D-s^{ex}$  scaling. The colloidal samples consisted of ellipsoidal (having aspect ratio  $p = 1.26, 1.60, 1.84, 2.68, 3.72, 5.00, \text{ and } 7.06$ , see Supplementary Fig. 1) or binary spherical particles. We found that the  $D-s^{ex}$  scaling broke down for glass-forming liquids at unexpectedly low area fractions. Accompanying the breakdown, we observed enhanced translation–rotation coupling and a topography change of the FEL. Further analysis of relaxation time indicated a positive correlation between the fragility of a liquid and the area fraction ( $\phi_T$ ) at which the  $D-s^{ex}$  scaling broke down. Our experiments shed light on the study of molecular glasses and emphasised the crucial role that thermodynamical entropy plays in the kinetic slowdown during glass transition.

## Results

**Kinetic pathways and  $D-s^{ex}$  scaling.** As the area fraction increases, a liquid (Supplementary Fig. 2a) can undergo one of two kinetic pathways. One path (c-path) entails crystallising into an ordered solid (Supplementary Fig. 2b) through a thermodynamic phase transition. When crystallisation of a system is suppressed either through rapid cooling or through incompatible motif symmetry, however the system’s glass transition intervenes<sup>2</sup> (Supplementary Fig. 2c). The glass transition is abbreviated as ‘g-path’ in this paper. In our experiments, spheres were able to follow c-path as well as ellipsoids with  $p = 1.26$ ; however, binary and other ellipsoids tended to follow the g-path. To more clearly express our experimental system in the language of glass transition, we extracted  $\phi_g$  by calculating the intermediate scattering function  $F_s(\mathbf{q}, t) = \langle \sum_{j=1}^N e^{i\mathbf{q} \cdot (\mathbf{x}_j(t) - \mathbf{x}_j(0))} \rangle / N$  (Fig. 1a). Here,  $\mathbf{x}_j(t)$  represents the position of ellipsoid  $j$  at time  $t$ ,  $\mathbf{q}$  is the scattering vector,  $N$  is the total number of particles, and  $\langle \rangle$  denotes the ensemble average. We chose  $q = q_m$  corresponding to the first peak in the structure factor at high density. The relaxation time ( $\tau_\alpha$ ) was then defined as the time at which  $F_s(\mathbf{q}, t)$  had decayed to  $1/e$  (dotted line in Fig. 1a). Subsequently, we plotted  $1/\tau_\alpha$  as a function of  $\phi$  and then extrapolated  $1/\tau_\alpha$  to zero (Fig. 1b) with the equation  $1/\tau_\alpha = (\phi_g - \phi)^\gamma$ . The relaxation time, according to this formula, must diverge at  $\phi_g$ , which serves as the glass transition point of the system. Our fitted  $\phi_g$  (Fig. 1c) decreased with the aspect ratio, and the values were consistent with those reported in other colloidal experiments<sup>6,39</sup>.

In colloidal experiments, determining the full value of excess entropy is difficult. The two-body part of excess entropy ( $s_2^{ex}$ ) has been reported to contribute more than 70% of  $s^{ex}$  and to have a linear relationship with  $s^{ex}$ , identified using simulations<sup>32,40</sup>.

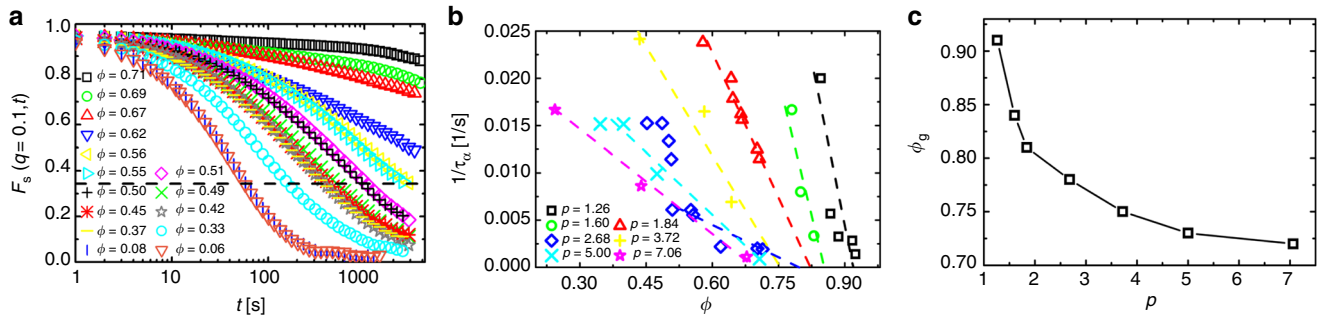


**Fig. 1** Glass transition point. **a** The intermediate scattering function,  $F_s(\mathbf{q}, t)$ , of the ellipsoid with  $p = 2.68$ . The relaxation time was defined as the time at which  $F_s(\mathbf{q}, t)$  decayed to the value  $1/e$  (dashed horizontal line). **b** The inverse of the relaxation time as a function of the area fraction for all glass-forming liquids composed of ellipsoid particles. The glass transition points ( $\phi_g$ ) were determined by extrapolating (dashed lines) the inversed relaxation time to zero. **c** The  $\phi_g$  of ellipsoids as a function of  $p$

Thus, we abbreviate  $s_2^{ex}$  as  $s_2$  in brief to identify a specific quantity to test the slowdown kinetics. The two-body excess entropies in the translational and rotational degrees of freedom were evaluated according to the following equations<sup>6,41</sup>:

$$s_2^T = -\pi k_B \rho \int_0^{+\infty} [g(r) \ln g(r) - g(r) + 1] r dr \quad (1)$$

$$s_2^\theta = -\frac{1}{2} k_B \rho \int_0^{+\infty} g(r) r dr \int_0^{2\pi} g(\theta|r) \ln [g(\theta|r)] d\theta \quad (2)$$

where  $k_B$  is the Boltzmann constant,  $\rho$  is the number density,  $g(r)$  is the radial distribution, and  $g(\theta|r)$  is the orientation distribution function of the angular difference between the long axes at some distance  $r$ . The long-time diffusion coefficient ( $D$ ) used in the rest of this manuscript was the slope of the ‘out-of-cage’ part of the mean square displacement (Supplementary Fig. 3) obtained through linear fitting.

Regarding the rotational degree of freedom, the  $D^\theta - s_2^\theta$  scaling held for all ellipsoids (Fig. 2a) when  $\phi$  ranged nearly all the way up to the orientational glass transition point<sup>6</sup>, after which the long-time diffusion coefficient vanished. The  $D^\theta - s_2^\theta$  data for rotational motion were adequately fitted by the exponential decay  $D^\theta \sim e^{-\alpha s_2^\theta}$ . It is noteworthy that a sudden jump of the fitted exponent  $\alpha$  occurred between  $p = 3.27$  and  $p = 5.00$ . Because  $\alpha$  reflects how fast the kinetics of the system slows down after losing the same number of available configurations, lower  $\alpha$  value for small  $p$  ellipsoids implied milder and probably continuously increasing non-ergodicity as a function of  $\phi$ <sup>15,16</sup>. This finding coincided well with previous molecular dynamics simulations and thus provided experimental verification of the proposed weak steric hindrance scenario for the slightly elongated particles<sup>15,16</sup>.

The situation for the translational degree of freedom was qualitatively different. We found that for all liquids that follow the c-path (spheres and  $p = 1.26$  ellipsoids), the  $D^T - s_2^T$  scaling in the translation was valid (Fig. 2c, d) for area fractions ranging from 0.05 to 0.70. However, the  $D^T - s_2^T$  scaling broke down for g-path liquids (binary and all ellipsoids) at surprisingly low area fractions ( $\phi_T$ ) (Fig. 2) relative to  $\phi_g$  (Fig. 1c). When  $\phi$  was higher than  $\phi_T$ , the kinetics of glass-forming liquids slowed down much more rapidly than the kinetics of the liquids that crystallised. Interestingly, for  $p = 1.26$  ellipsoids, we discerned a bifurcated pattern in the  $D^T - s_2^T$  plot (Fig. 2d). Raw images depict that the  $p = 1.26$  ellipsoid crystallised (right inset of Fig. 2d) or formed glass (left inset of Fig. 2d) depending on the wall separation of the samples (Supplementary Fig. 2 and Supplementary Note 1). Consistently, the samples following the c-path obeyed the normal  $D^T - s_2^T$  scaling whereas the samples following the g-path

deviated from the exponential fitting (dashed lines in Fig. 2d). On the basis of these observations, we concluded that the breakdown of  $D^T - s_2^T$  scaling was caused by glassy effects.

There existed a turning point, which was defined as the first point in the  $D^T - s_2^T$  plots (Fig. 2c, d) that deviated from the exponential fitting (dashed line in Fig. 2c-e); this point thus separated the smooth and rapid slowdown processes in the translational degree of freedom for each g-path liquid. The raw images that correspond to the turning points and the area fractions ( $\phi_T$ ) are presented in Fig. 3. Unexpectedly,  $\phi_T$  covered a wide  $\phi$  range from 0.13 to 0.72 for various g-path liquids. For binary (Fig. 3a and Supplementary Figs. 6, 8a and 9a) and other ellipsoids<sup>6,7</sup> (Fig. 3c-h),  $\phi_T$  was considerably lower than the onset of DH (Supplementary Figs. 6-9), whereas for the  $p = 1.26$  ellipsoid (Fig. 3b),  $\phi_T$  was higher than the area fraction at which DH occurs<sup>7</sup> (Fig. 3b and Supplementary Figs. 5, 8b and 9b). Therefore, any turning in the  $D^T - s_2^T$  scaling should have been irrelevant to DH (see more discussions in Supplementary Note 2). The properties, such as  $\phi_T$ , of the transient region between the liquid and glass states have usually been overlooked by current dynamic theories in part because the density of a system in this region is apparently too low to allow any DH to occur. Instead of DH, three major features of the system at  $\phi_T$  are reported in the following sections.

**Abnormal translational-rotational cross-correlation at  $\phi_T$ .** We observed that the abnormal coupling between translation and rotation was significantly enhanced at  $\phi_T$ . For systems composed of anisotropic-shaped particles such as ellipsoids<sup>6</sup> or dumbbells<sup>42</sup>, the translational and rotational motions were no longer independent whenever a collision occurred. Such systems are usually also effective glass formers. However, the relationship between  $\phi$  and collision frequency, which can be calculated from the height of the first peak of the radial distribution function  $g(r)$ <sup>19,20</sup>, can be complicated if a system takes its g-path. For a strong glass former in particular, the shape of  $g(r)$  minimally changes with increasing  $\phi$  (Supplementary Fig. 18c)<sup>43</sup>. Therefore, how the enhanced translational-rotational correlation affects the kinetic pathway and eventually alters the  $D^T - s_2^T$  scaling remains unexplored.

To characterise the translation-rotation coupling, we defined the cross-correlation function for ellipsoidal particles as  $C_{xy\theta}(t) = 2\langle \Delta x \Delta y \rangle \langle \sin 2\theta \rangle / t$ , where  $\Delta x$  and  $\Delta y$  are displacements in time period  $t$  in the  $x$  and  $y$  directions, respectively;  $\theta$  is the angle of an ellipsoid (in the lab frame) at time  $t$ , and the angle brackets represent the ensemble average. For a single ellipsoid diffusing in water, the friction coefficient parallel to the major axis is invariably smaller than that which is perpendicular to the major axis, resulting in positive translation-rotation coupling in the lab



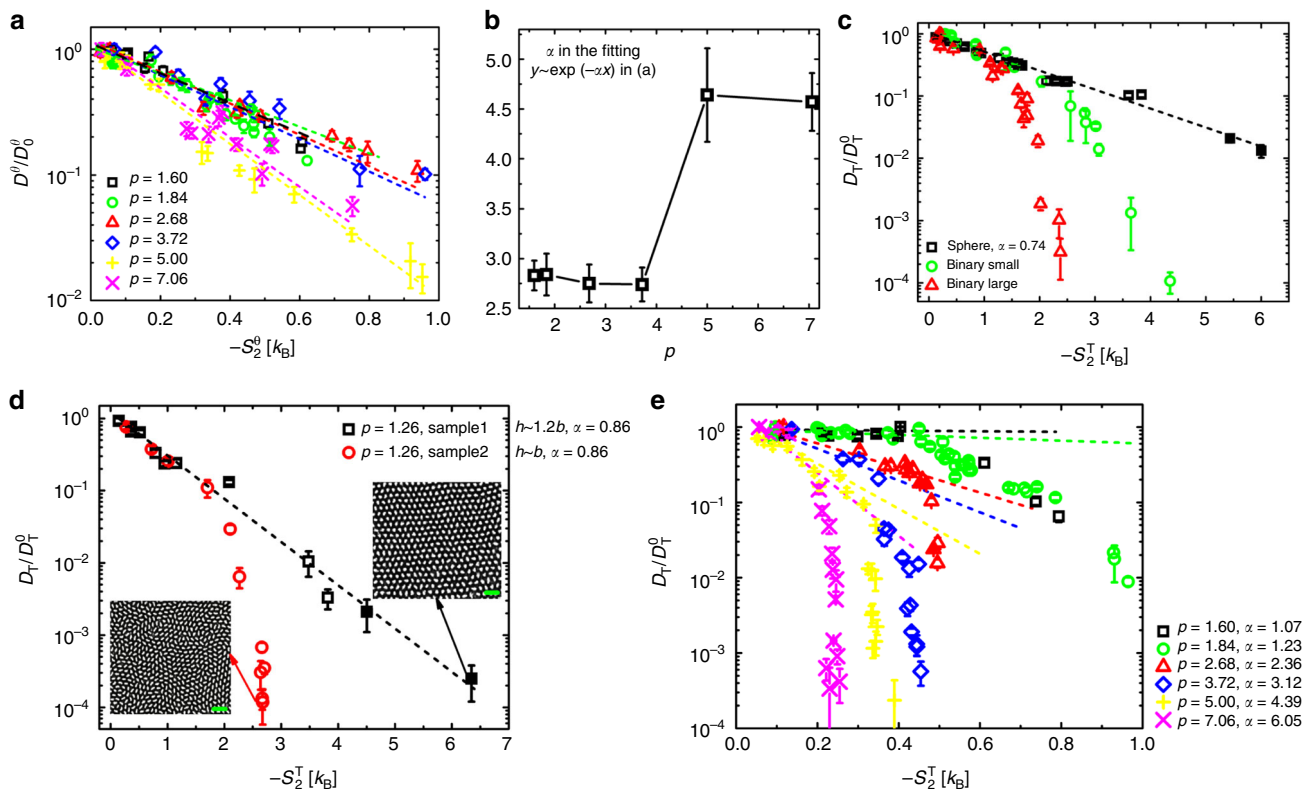


**Fig. 2** Relationship between diffusion coefficient and two-body excess entropy. **a** the  $D^\theta - s_2^\theta$  relationship for the rotational motion of ellipsoids with aspect ratios ranging from 1.60 to 7.06. The fitted decay exponential is presented in **b**. The data for the  $p = 1.26$  ellipsoid is missing because the determination of the particles' orientation was inaccurate when they tilted in z-direction. Compared with the case of monodispersed spherical particles in **c**, the exponential scaling for translational motion ( $D^T \sim e^{-\alpha s_2^T}$ ) breaks down at certain points for binary spherical (**c**) and ellipsoidal (**d, e**) systems. The fitted decay exponential  $\alpha$  is presented in the legend of the figures accordingly. In particular, **d** demonstrates the bifurcation of the  $D^T - s_2^T$  relation for a small-aspect-ratio ( $p = 1.26$ ) ellipsoid system, which either crystallises (right inset of **d**) or vitrifies (left inset of **d**), depending on the sample thickness ( $h$ ). The solid points in **c, d** denote that the samples crystallise from their liquid states. The scale bar is  $10 \mu\text{m}$ . The dashed lines are fitted to the relation  $D \sim e^{-\alpha s_2}$ . The diffusion coefficients were determined by fitting the mean square displacement data in long time into linear form. The errors were the standard deviation (scaled by  $D_0$ ) of the slopes

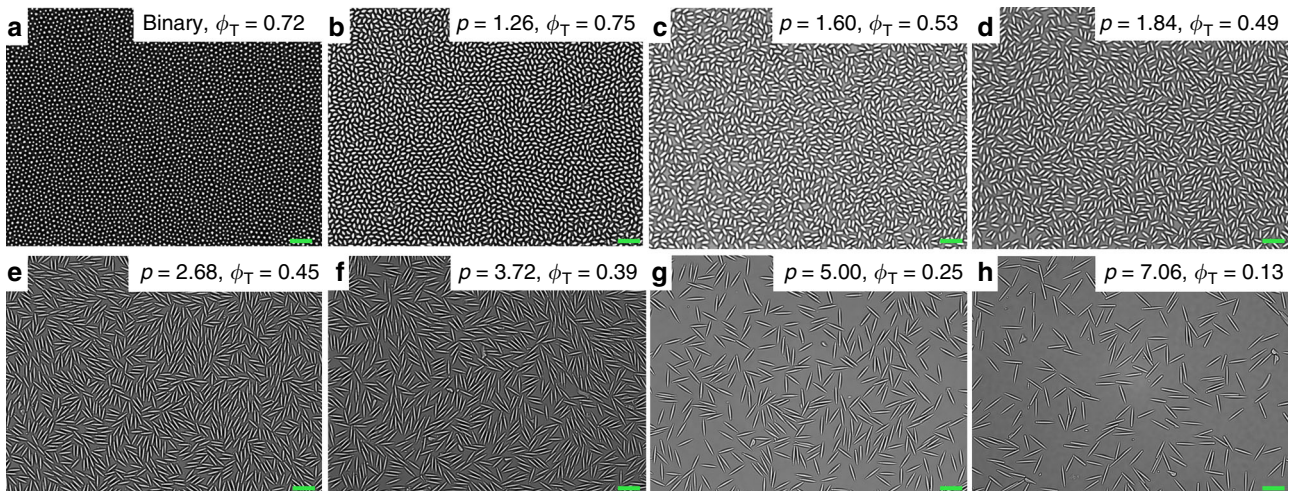


**Fig. 3** Raw images captured at the turning points of the translational  $D^T - s_2^T$  plots. The area fractions ( $\phi_T$ ) corresponding to the turning points for **a**, binary spherical, **b**,  $p = 1.26$ , **c**,  $p = 1.60$ , **d**,  $p = 1.84$ , **e**,  $p = 2.68$ , **f**,  $p = 3.72$ , **g**,  $p = 5.00$  and **h**,  $p = 7.06$  ellipsoidal systems are specified in each figure. The scale bar is  $5 \mu\text{m}$

frame<sup>44</sup>. If an ellipsoid particle is in a crowded environment such as a suspension of high-density active bacteria, however, negative cross-correlation may be evident<sup>45</sup>. In our experiments, we observed four types of cross-correlation in total (Fig. 4a). In

addition to the normal case for a single Brownian ellipsoid (the black curve in Fig. 4a), the other three types were abnormal because of negative correlations during certain time periods. The green dash-dotted curve exhibiting only a negative part was

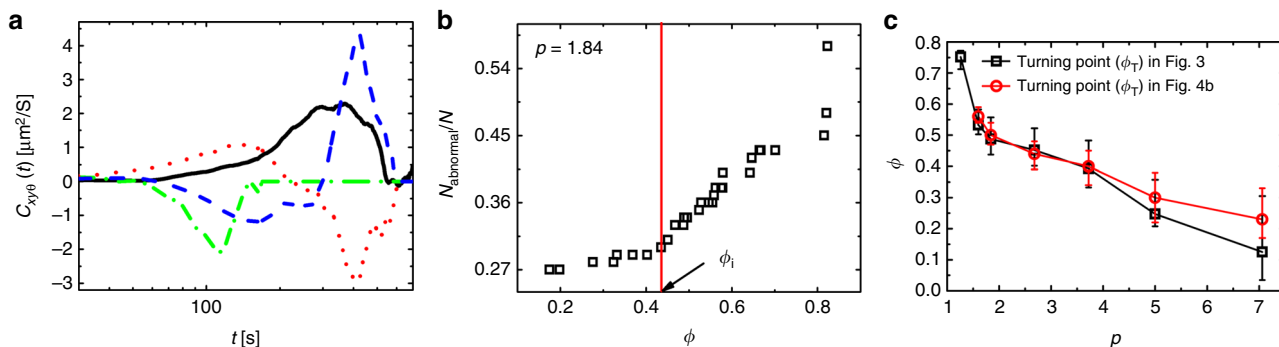


**Fig. 4** Abnormal cross-correlation in ellipsoid systems. **a** Four types of cross-correlation  $C_{xy\theta}(t)$  in ellipsoid systems. **b** The fraction of abnormally correlated (red-dot, blue-dash, and green-dash-dot lines in **a**) particles as a function of area fraction starts to increase at  $\phi_i$ . **c** Area fraction corresponding to the turning point ( $\phi_T$ ) in  $D^T - s_2^T$  plots and enhanced abnormal correlation ( $\phi_i$  in **b**)

caused by non-central collisions between only two particles, which solely enhanced motion in the direction perpendicular to the long axis. The other two curves exhibiting both positive and negative parts likely involved multi-particle collision events that caused opposite effects the motion of the particles at various time scales.

We counted the number of fractions of particles that exhibited abnormal cross-correlation for each  $\phi$  and for all seven types of ellipsoids and determined that the proportion of abnormal particles started to increase considerably at certain area fractions  $\phi_i$  (Fig. 4b). In addition,  $\phi_i$  coincided favourably with  $\phi_T$  within the experimental accuracy (Fig. 4c). As previously discussed, the negative  $C_{xy\theta}(t)$  was caused by abnormally slow diffusion along the major axis, which is strictly prohibited for a single Brownian ellipsoid. As  $\phi$  increased, the abnormal diffusion could thus only have been generated by increasingly frequent collisions among particles. Thus, the booming ratio of particles with abnormal cross-correlation at  $\phi_i$  was an effective indicator of enhanced collision frequency within the system. In other words,  $\phi_i$  was also the point at which particles started to collide frequently. Thus, it seemed that the observed abnormal cross-correlation strongly indicated that the microscopic origin causing the breakdown of  $D^T - s_2^T$  scaling in ellipsoidal systems could be deeply rooted in the translation-rotation coupling caused by noncentral collisions among particles.

Nonetheless, if the turning in  $D^T - s_2^T$  scaling was solely caused by translation-rotation coupling, it should have commonly existed for both degrees of freedom, but that was not what was observed in the experiments (Fig. 2a). The absence of turning in the rotational degree of freedom, as well as the existence of turning in binary systems creates ambiguity with respect to the role played by collision in the turning. A new theoretical definition of pairwise entropy that combines the translational and rotational motions may offer superior insight into the role played by their coupling. In addition, it is questionable whether the short-timescaled (approximately 100 s in Fig. 4a) cross-correlation (or collisions) would be able to influence the relaxation of glasses at much longer timescales ( $>1000$  s). Therefore, the roles that noncentral collisions and translation-rotation coupling play in the kinetic slowdown of ellipsoidal systems remain undetermined and warrant further investigation.

**Rugged FEL topography near  $\phi_T$ .** Another feature of the turning is the rugged FEL topography near  $\phi_T$ . For a system with  $N$  particles, the FEL is a  $6^N$  hypersurface, which is hardly calculable when  $N$  is large<sup>46</sup>. In practice, it was proven by simulation that the topography of FEL can be approximately depicted by average particle

mobility<sup>47-49</sup>. Herein, we express the mobility in translational motion as  $\Delta u(t) = \left(\frac{1}{N}\right) \sum_{i=1}^N [\mathbf{u}_i(t + \tau_\alpha/2) - \mathbf{u}_i(t - \tau_\alpha/2)]$ , where  $N$  is the particle number,  $\tau_\alpha$  is the relaxation time (defined in Fig. 1a), and  $\mathbf{u}_i$  is particle  $i$ 's displacement at a given time<sup>47-49</sup>. Simulations have suggested that over a much broader  $\phi$  range than the range in which MCT takes effect, the relaxation kinetics are mainly sensitive to the topography of the FEL<sup>46,48-50</sup>, implying that inherent structure is a useful tool for predicting glassy kinetics when the density of the system is low. In Fig. 5a-c we display the time dependence of  $\Delta u(t)$  for the  $p=5.00$  ellipsoid under three typical area fractions. Compared with the FEL at low density (Fig. 5a), the topography of the FEL in translational motion became rugged in the vicinity of  $\phi_T$  (Fig. 5b) and thereafter (Fig. 5c). By contrast, the topography of the FEL in rotational motion,  $\Delta \theta(t) = \left(\frac{1}{N}\right) \sum_{i=1}^N [\theta_i(t + \tau_\alpha/2) - \theta_i(t - \tau_\alpha/2)]$ , remained smooth over the whole  $\phi$  range (Fig. 5d-f), agreeing with the absence of a turning in the  $D^\theta - s_2^\theta$  plot (Fig. 2a). Without exception, the standard binary system exhibited rugged FEL near  $\phi_T$  (Fig. 5g-i). More quantitative analysis of FEL was conducted by calculating the probability distribution of the mobility and its half width in Supplementary Note 3 (Supplementary Fig. 17). A sudden jump of the half-width for translational motion occurred at  $\phi_T$  and a similar jump for rotational motion occurred much later (Supplementary Fig. 17c). This measurement unambiguously suggested that ellipsoid particles were still free to rotate at the  $\phi$  when translational motion began to be caged, in accordance with caging sequence predicted by simulation and MCT<sup>15,16</sup>. The evolution of the FEL topographies of all other g-path liquids exhibited tendencies (Supplementary Figs. 11-16) similar to those depicted in Fig. 5 and Supplementary Fig. 17. These observations confirmed the major role that inherent structures play in  $D - s_2$  scaling.

However, the fact that both rugged FEL and  $D^T - s_2^T$  turning (i.e.  $\phi_T$ ) occurred much earlier than DH appeared to support the simulation results that rugged FEL occurred much earlier than the transition point predicted by MCT<sup>50</sup>. This 'overlook' by MCT indicated that the turning we observed in the low-density region probably deeply involved in thermodynamic or dynamical fluctuations rather than mean field properties. Confirming the causal role FEL plays in the breakdown of  $D^T - s_2^T$  scaling required a more direct means of accessing inherent structures in phase space than the current analysis using mobility representation.

Near  $\phi_T$ , some adjacent inherent structures formed basins on larger time scales (Fig. 5b, c), during which the system was trapped within a small number of inherent structures. The presence of this substructure in the FEL reflected the highly nontrivial nature of the entire hypersurface that resulted from many-body interactions<sup>51</sup>. When  $\phi$  was high, the presence of

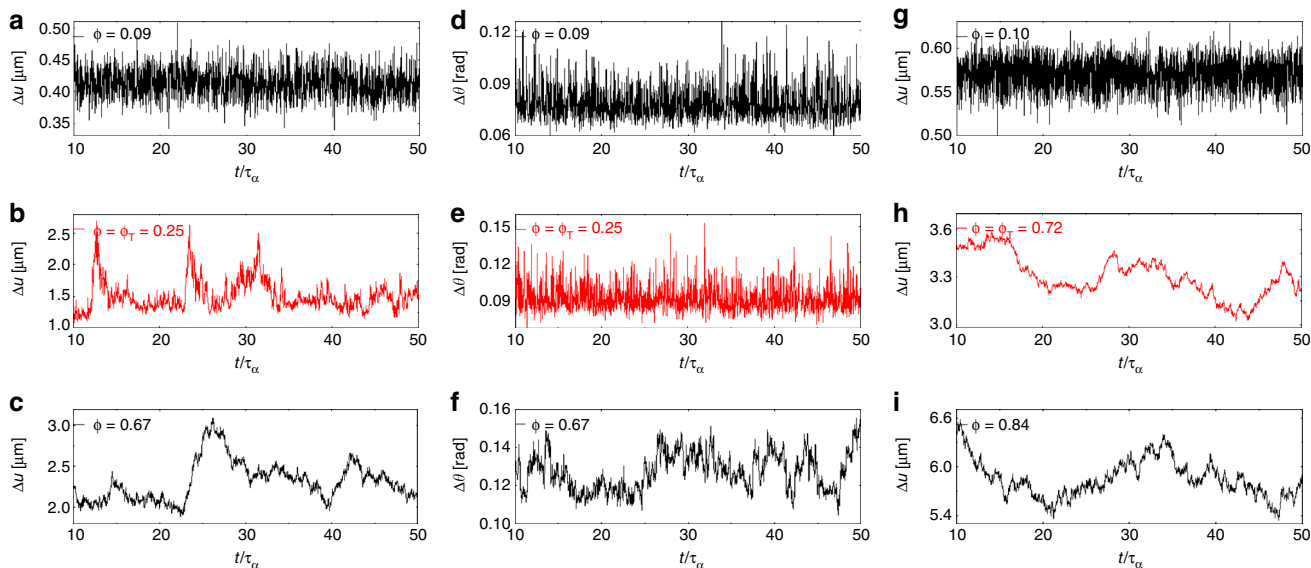


**Fig. 5** Topography of the free energy landscape (FEL) in representation of particle mobility. For the  $p = 5.00$  ellipsoid system, we chose **a**,  $\phi = 0.09$ ; **b**,  $\phi = \phi_T = 0.25$  and **c**,  $\phi = 0.67$  samples and calculated the time evolution of their translational displacements,  $\Delta u(t)$ , during the relaxation time  $\tau_\alpha$ . The rotational displacements  $\Delta\theta(t)$  under the same  $\phi$  are presented in **d–f**. The translational displacements of binary samples with **g**,  $\phi = 0.10$ ; **h**,  $\phi = \phi_T = 0.72$  and **i**,  $\phi = 0.84$  are also presented. The term  $\tau_\alpha$  is defined as the time at which the intermediate scattering function has decayed to  $1/e$

valleys dramatically slowed down the kinetics and was thus the limiting step for full structural relaxation. During residence in a basin, the configuration fluctuated only slightly and thus corresponded to a long-lived metastable state that abrogated the ergodicity of the system. High activation energy was required for the system to relax from one basin to another<sup>52</sup>. Increasingly few configurations were available after  $\phi_T$ . Consequently, when  $\phi$  increased, the loss of configurations (or entropy,  $s_2^T$ ) caused the kinetics to more violently slow down ( $D^T$ ) compared with the situation before  $\phi_T$ . When  $\phi$  was low, however, the residence probability in the configuration space was no longer dominated by the regions around the inherent structures; therefore, no stationary inhomogeneous density field could be defined over periods longer than microscopic times<sup>52</sup> and the kinetics became irrelevant to the topography of the FEL<sup>13</sup>.

**Positive correlation between fragility and  $\phi_T$ .** A crucial feature of  $\phi_T$  is its connection with fragility ( $m$ ), which is another quantity that reflects the inherent character of the FEL<sup>2</sup>. To determine the fragility of a liquid, we produced Arrhenius plots of relaxation time as a function of the area fraction scaled by values of  $\phi_g$  (Fig. 6a). Fragility  $m$  was then defined as the derivative of the scaled relaxation time as a function of the area fraction scaled by  $\phi_g$  as  $m = \left. \frac{\partial(\tau_\alpha/\tau_\alpha^0)}{\partial(\phi/\phi_g)} \right|_{\phi=\phi_g}$  53.

As is evident in Fig. 6b, both  $m$  and  $\phi_T$  decreased with the aspect ratio. Without exception, the data from the binary system conformed to this tendency. Thus the striking differences between fragile and strong liquids can be directly evaluated using the  $D^T - s_2^T$  scaling (Fig. 2c–e). The kinetic slowdown of a strong liquid begins to deviate from the form  $D \sim e^{-\alpha s^{\text{ex}}}$  at a much lower  $\phi_T$  than a fragile liquid. A molecular dynamics (MD) simulation demonstrated that when  $\phi$  increased,  $D$  decayed faster for strong liquids than for fragile liquids<sup>54</sup>. Our observations provided clear experimental support to this finding (Fig. 2e). The difference between strong and fragile liquids can also be evaluated from the structural reaction of a liquid towards cooling. Typically, a stronger

liquid exhibits less structural change within the same temperature range<sup>55</sup>. Supplementary Fig. 18 illustrates that for a similar range of diffusion coefficients, decreasing from  $1$  to  $10^{-3}$ , the first peak of the radial distribution function ( $g(r)$ ) for fragile liquids altered correspondingly (Supplementary Fig. 18a, b, d) but hardly changed for strong liquids (Supplementary Fig. 18c, d). Evidence was also apparent that the first peak of  $g(r)$  saturated at  $\phi_T$ .

The unambiguously positive correlation between  $\phi_T$  and  $m$  (Fig. 6b) highlighted the crucial role of  $\phi_T$  in glass transitions. We determined that a g-path liquid tends to exhibit a continuous transformation from fast relaxation in the low  $\phi$  region to slow relaxation in the high  $\phi$  region (Fig. 6a). The transformation usually occurs at lower  $\phi$  regions for strong liquids than for fragile liquids. This explains why  $\phi_T$  was lower for ellipsoids with larger  $p$ -values, or equivalently, stronger liquids in our experiments (Figs. 2b–d and 6b). In addition, because a liquid's relaxation is characterised by  $m$  in the thermodynamic picture, the relaxation of a g-path liquid at a high  $\phi$  can be precisely predicted by measuring its  $D^T - s_2^T$  relation and identifying  $\phi_T$ . Unlike  $\phi_g$ ,  $\phi_T$  usually lies well within the liquid region. Therefore,  $\phi_T$  should be useful for probing glassy behaviours that are typical of much higher  $\phi$  while circumventing the prohibitive increase in equilibration times.

The slowdown kinetics after  $\phi_T$  were also directly related to  $m$  and could be understood from the visualisations of FEL<sup>13</sup>, in which the variation between behaviours of the strong and fragile liquids was tracked back to topographic differences in the FEL. The extremes of strong glass formers ( $p = 3.72, 5.00$ , and  $7.06$  ellipsoids in our experiments, Fig. 6a) presented a uniformly rough topology, exhibiting little or no coherent organisation of individual basins into large and deep craters<sup>13</sup>. The relaxation of the system was dominated by jumps among a few isolated local minima (basin of attraction) in a single energy-scaled FEL<sup>46,47</sup>. In other words, the configurations in which the system could dwell were dearth for a strong liquid. As the area fraction increased, the local minima became deeper and the relaxation between any two minima required overcoming an increasingly high energy barrier. The system remained within one local minimum. Therefore, the



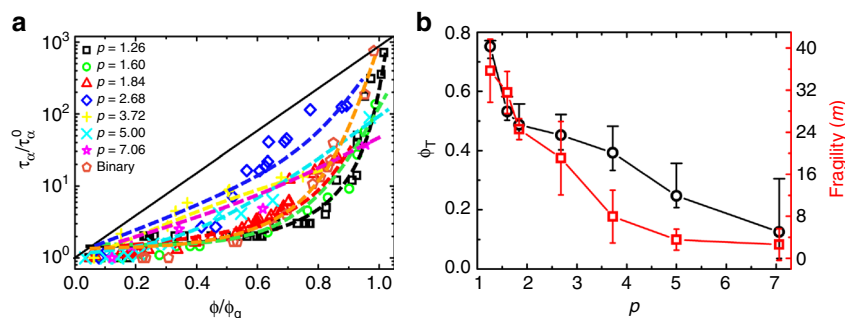


**Fig. 6** Fragility and  $D^T - s_2^T$  turning. **a** Arrhenius plots of relaxation time as functions of the area fraction scaled by  $\phi_g$ . The solid black line and the dashed lines are to enhance viewing. **b** Both the fragility ( $m$ ) and turning point ( $\phi_T$ ) of the  $D - s_2$  relation decreased with the aspect ratio. The errors of  $\phi_T$  and  $m$  came from the standard deviations of the fitting parameters

loss of local minima (or entropy) upon cooling led to much faster slowdown of the kinetics of a strong liquid (Fig. 6a), which is reflected by the steeper  $D^T - s_2^T$  scaling after  $\phi_T$  in Fig. 2e.

## Discussion

In summary, we have reported the systematic experimental study of kinetic slowdown of colloidal glass-forming liquids from the perspective of thermodynamics<sup>56,57</sup>. We found the  $D^T - s_2^T$  scaling for all  $g$ -path liquids turned at fairly low area fractions ( $\phi_T$ ), which defined a new ‘transition’ point that had not been addressed previously. After  $\phi_T$ , the slowdown process was greatly accelerated. This finding demonstrates the crucial role thermodynamic entropy plays in kinetic slowdown. In addition, profound interactions were evident between kinetic slowdown, translation–rotation coupling, FEL topography, and fragility. We expect results similar to ours to be observed in other systems, both in 2D and 3D where crystallisation is depressed such as polydispersed colloidal systems<sup>58</sup>, granular systems<sup>22</sup>, emulsion droplet systems<sup>59</sup> and even cellular systems<sup>60</sup>, because the general rule that controlled the slowdown of kinetics approaching the glass transition should be the same.

The most challenging task associated with this research was how to integrate our observations with current theoretical frameworks<sup>1</sup>. Although they did not conflict with any well-established model, most of our observations had not been addressed by established theories. The turning point ( $\phi_T$ ) proposed in this article had been proven to be irrelevant with the onset of DH (Fig. 3 and Supplementary Figs. 5–9) and was too low to attract any attention in the previous theories<sup>1</sup>. At  $\phi_T$ , the relaxation of the system was dominated by few-particle dynamics without diverging static or dynamical length scales. The turning itself was therefore not related to the collective glassy dynamics. Meanwhile, our findings strongly indicate that behaviours of the low-density liquids can foreshadow the kinetic paths and relaxation phenomena of their high-density counterparts, namely, glasses. Because previous simulations demonstrated that  $\phi_g$  also scaled with the jamming packing fraction ( $\phi_j$ )<sup>61,62</sup> and we found that  $\phi_g$  as a function of  $\phi_T$ , could be fitted by a stretched exponential (Supplementary Fig. 19 and Supplementary Note 4), it would seem reasonable to expect that the turning also has some relation to the jamming transition. Therefore, the connection between behaviours at various time and length scales—liquid, glass and jammed states—remains an interesting open question. To investigate this, theories such as the self-consistent generalised Langevin equation<sup>63</sup> may play a role because the multi-length scale needs to be taken into consideration. Moreover, since  $\phi_T$  is essentially a ‘blended’ quantity that is determined by the joint

effect of entropy and the diffusion coefficient, it would be worthwhile to investigate interactions between thermodynamics and kinetics in theory.

The reason why the FEL topographies in various degrees of freedom are so distinct has yet to be fully explored. Our data (Fig. 5a–f and Supplementary Figs. 12–16) demonstrate that the FEL in translational motions became rugged in advance of rotational motions, which suggested the ellipsoids were still free to rotate when they were already non-ergodic in translation. This caging sequence support the previous results of MD simulations<sup>15,16</sup> where two glass transition lines were identified in the dynamical phase diagram. In addition, the jump in the decay exponent of  $D^\theta - s_2^\theta$  in Fig. 2b, as well as the sharp decrease of  $\phi_T$  (Fig. 6b) as a function of  $p$  indicated qualitatively distinct glass transitions for small and large  $p$  ellipsoids because of different translation–rotation couplings. It would therefore be meaningful to undertake more quantitatively comparative experiments and simulate data to investigate the characteristics of strong and weak steric hindrance scenarios. Our current experiments have paved the way for establishing a link between random first-order transition theory and inherent structure.

## Methods

In this experiment, we used two types of colloidal glass-forming liquids that consisted of ellipsoidal or binary spherical particles. For the ellipsoidal system, we stretched polymethyl methacrylate (PMMA) spheres (Microparticles GmbH, Germany) with a diameter of  $\sigma = (2.74 \pm 0.04) \mu\text{m}$  into ellipsoid particles with aspect ratios  $p = a/b = 1.26, 1.60, 1.84, 2.68, 3.72, 5.00$ , and  $7.06$  and polydispersity of less than 5%. Here,  $a$  and  $b$  were the major and minor axes, respectively. For the binary spherical system, we mixed  $\sigma = (2.08 \pm 0.05) \mu\text{m}$  and  $2.74 \mu\text{m}$  PMMA spheres homogeneously with a ratio of 0.55:0.45. The particles underwent short-ranged repulsive interaction. Both the ellipsoidal and binary spherical systems effectively avoided crystallisation and thus served as satisfactory glass formers. The ellipsoids with  $p = 1.26$  sometimes formed rotator crystals<sup>6</sup> when the wall separation was appropriate, but they formed glass in most trails. We also used  $2.74 \mu\text{m}$  PMMA mono-dispersed spheres for a control group. To optimally image and track particle motion, we adopted a quasi-two-dimensional sample configuration in which colloidal particles were dispersed in water between two parallel horizontal glass walls that had a separation of less than  $1.2 \sigma$ , and screened off the majority of the hydrodynamic force between particles<sup>24</sup>. For colloids in 2D, the area fraction  $\phi = \pi ab\rho$  played the same role as the inverse temperature  $1/T$  plays in molecular systems and  $\rho$  represents the number density. Approximately 10 to 25 area fractions within  $0.02 \leq \phi \leq 0.95$  were recorded for each aspect ratio through video microscopy. During the 2- to 4-h measurements at each  $\phi$ , no drift, flow, or density change were observed. The center-of-mass positions and orientations of 200–5000 ellipsoids were tracked using an image-processing algorithm<sup>36</sup>.

## Data availability

The data supporting the findings of this study are available from the corresponding authors upon reasonable request.

Received: 20 June 2018 Accepted: 19 October 2018

Published online: 09 November 2018

## References

- Berthier, L. & Biroli, G. Theoretical perspective on the glass transition and amorphous materials. *Rev. Mod. Phys.* **83**, 587–645 (2011).
- Angell, C. A. et al. Formation of glasses from liquids and biopolymers. *Science* **267**, 1924–1935 (1995).
- Kirkpatrick, T. & Thirumalai, D. Colloquium: random first order transition theory concepts in biology and physics. *Rev. Mod. Phys.* **87**, 183–209 (2015).
- Keys, A. S., Hedges, L. O., Garrahan, J. P., Glotzer, S. C. & Chandler, D. Excitations are localized and relaxation is hierarchical in glass-forming liquids. *Phys. Rev. X* **1**, 021013 (2011).
- Zhang, Z., Yunker, P. J., Habdas, P. & Yodh, A. Cooperative rearrangement regions and dynamical heterogeneities in colloidal glasses with attractive versus repulsive interactions. *Phys. Rev. Lett.* **107**, 208303 (2011).
- Zheng, Z. et al. Structural signatures of dynamic heterogeneities in monolayers of colloidal ellipsoids. *Nat. Comm.* **5**, 3829–3840 (2014).
- Mishra, C. K. & Ganapathy, R. Shape of dynamical heterogeneities and fractional Stokes-Einstein and Stokes-Einstein-Debye relations in quasi-two-dimensional suspensions of colloidal ellipsoids. *Phys. Rev. Lett.* **114**, 198302 (2015).
- Golde, S., Palberg, T. & Schöpe, H. J. Correlation between dynamical and structural heterogeneities in colloidal hard-sphere suspensions. *Nat. Phys.* **12**, 712–717 (2016).
- Kob, W., Roldán-Vargas, S. & Berthier, L. Non-monotonic temperature evolution of dynamic correlations in glass-forming liquids. *Nat. Phys.* **8**, 164–167 (2012).
- Tanaka, H., Kawasaki, T., Shintani, H. & Watanabe, K. Critical-like behaviour of glass-forming liquids. *Nat. Mater.* **9**, 324–331 (2010).
- Shintani, H. & Tanaka, H. Frustration on the way to crystallization in glass. *Nat. Phys.* **2**, 200–206 (2006).
- Adam, G. & Gibbs, J. H. On the temperature dependence of cooperative relaxation properties in glass-forming liquids. *J. Chem. Phys.* **43**, 139–146 (1965).
- Stillinger, F. H. A topographic view of supercooled liquids and glass formation. *Science* **267**, 1935–1939 (1995).
- Stillinger, F. H. & Debenedetti, P. G. Glass transition thermodynamics and kinetics. *Annu. Rev. Condens. Matter Phys.* **4**, 263–285 (2013).
- Chong, S. H., Moreno, A. J., Sciortino, F. & Kob, W. Evidence for the weak steric hindrance scenario in the supercooled-state reorientational dynamics. *Phys. Rev. Lett.* **94**, 215701 (2005).
- Moreno, A. J., Chong, S. H., Kob, W. & Sciortino, F. Dynamic arrest in a liquid of symmetric dumbbells: reorientational hopping for small molecular elongations. *J. Chem. Phys.* **123**, 204505 (2005).
- Kob, W. & Berthier, L. Probing a liquid to glass transition in equilibrium. *Phys. Rev. Lett.* **110**, 245702 (2013).
- Sastry, S. The relationship between fragility, configurational entropy and the potential energy landscape of glass-forming liquids. *Nature* **409**, 164–167 (2001).
- Dzugutov, M. A universal scaling law for atomic diffusion in condensed matter. *Nature* **381**, 137–139 (1996).
- Chapman, S., Cowling, T. & Park, D. The mathematical theory of non-uniform gases. *J. Am. Phys.* **30**, 389–389 (1962).
- Hoyt, J., Asta, M. & Sadigh, B. Test of the universal scaling law for the diffusion coefficient in liquid metals. *Phys. Rev. Lett.* **85**, 594–597 (2000).
- Wang, C. H., Yu, S. H. & Chen, P. Universal scaling laws of diffusion in two-dimensional granular liquids. *Phys. Rev. E* **91**, 060201 (2015).
- Samanta, A., Ali, S. M. & Ghosh, S. K. Universal scaling laws of diffusion in a binary fluid mixture. *Phys. Rev. Lett.* **87**, 245901 (2001).
- Ma, X. et al. Test of the universal scaling law of diffusion in colloidal monolayers. *Phys. Rev. Lett.* **110**, 078302 (2013).
- Thorneywork, A. L., Rozas, R. E., Dullens, R. P. & Horbach, J. Effect of hydrodynamic interactions on self-diffusion of quasi-two-dimensional colloidal hard spheres. *Phys. Rev. Lett.* **115**, 268301 (2015).
- Rosenfeld, Y. Relation between the transport coefficients and the internal entropy of simple systems. *Phys. Rev. A* **15**, 2545–2549 (1977).
- Ito, K., Moynihan, C. T. & Angell, C. A. Thermodynamic determination of fragility in liquids and a fragile-to-strong liquid transition in water. *Nature* **398**, 492–495 (1999).
- Scala, A., Starr, F. W., La Nave, E., Sciortino, F. & Stanley, H. E. Configurational entropy and diffusivity of supercooled water. *Nature* **406**, 166–169 (2000).
- Errington, J. R. & Debenedetti, P. G. Relationship between structural order and the anomalies of liquid water. *Nature* **409**, 318–321 (2001).
- Liu, Y., Fu, J. & Wu, J. Excess-entropy scaling for gas diffusivity in nanoporous materials. *Langmuir* **29**, 12997–13002 (2013).
- Goel, G., Krekelberg, W. P., Errington, J. R. & Truskett, T. M. Tuning density profiles and mobility of inhomogeneous fluids. *Phys. Rev. Lett.* **100**, 106001 (2008).
- Banerjee, A., Sengupta, S., Sastry, S. & Bhattacharyya, S. M. Role of structure and entropy in determining differences in dynamics for glass formers with different interaction potentials. *Phys. Rev. Lett.* **113**, 225701 (2014).
- Dzugutov, M., Simdyankin, S. I. & Zetterling, F. H. Decoupling of diffusion from structural relaxation and spatial heterogeneity in a supercooled simple liquid. *Phys. Rev. Lett.* **89**, 195701 (2002).
- Lu, P. J. & Weitz, D. A. Colloidal particles: crystals, glasses, and gels. *Annu. Rev. Condens. Matter Phys.* **4**, 217–233 (2013).
- Li, B., Zhou, D. & Han, Y. Assembly and phase transitions of colloidal crystals. *Nat. Rev. Mater.* **1**, 15011–15023 (2016).
- Murray, C. A. & Grier, D. G. Video microscopy of monodisperse colloidal systems. *Annu. Rev. Phys. Chem.* **47**, 421–462 (1996).
- Nagamanasa, K. H., Gokhale, S., Sood, A. & Ganapathy, R. Direct measurements of growing amorphous order and non-monotonic dynamic correlations in a colloidal glass-former. *Nat. Phys.* **11**, 403–408 (2015).
- Mishra, C. K., Nagamanasa, K. H., Ganapathy, R., Sood, A. & Gokhale, S. Dynamical facilitation governs glassy dynamics in suspensions of colloidal ellipsoids. *Proc. Natl Acad. Sci. USA* **111**, 15362–15367 (2014).
- Zheng, Z. et al. Glass transitions in quasi-two-dimensional suspensions of colloidal ellipsoids. *Phys. Rev. Lett.* **107**, 065702 (2011).
- Martinez, L. & Angell, C. A thermodynamic connection to the fragility of glass-forming liquids. *Nature* **410**, 663–667 (2001).
- Baranyai, A. & Evans, D. J. Direct entropy calculation from computer simulation of liquids. *Phys. Rev. A* **40**, 3817–3822 (1989).
- Chopra, R., Truskett, T. M. & Errington, J. R. Excess entropy scaling of dynamic quantities for fluids of dumbbell-shaped particles. *J. Chem. Phys.* **133**, 104506 (2010).
- Steinhardt, P. J., Nelson, D. R. & Ronchetti, M. Bond-orientational order in liquids and glasses. *Phys. Rev. B* **28**, 784 (1983).
- Han, Y. et al. Brownian motion of an ellipsoid. *Science* **314**, 626–630 (2006).
- Peng, Y. et al. Diffusion of ellipsoids in bacterial suspensions. *Phys. Rev. Lett.* **116**, 068303 (2016).
- Heuer, A. Properties of a glass-forming system as derived from its potential energy landscape. *Phys. Rev. Lett.* **78**, 4051–4054 (1997).
- Büchner, S. & Heuer, A. Metastable states as a key to the dynamics of supercooled liquids. *Phys. Rev. Lett.* **84**, 2168–2171 (2000).
- Appignanesi, G., Fris, J. R., Montani, R. & Kob, W. Democratic particle motion for metabasin transitions in simple glass formers. *Phys. Rev. Lett.* **96**, 057801 (2006).
- Denny, R. A., Reichman, D. R. & Bouchaud, J.-P. Trap models and slow dynamics in supercooled liquids. *Phys. Rev. Lett.* **90**, 025503 (2003).
- Doliwa, B. & Heuer, A. What does the potential energy landscape tell us about the dynamics of supercooled liquids and glasses? *Phys. Rev. Lett.* **91**, 235501 (2003).
- Stillinger, F. H. & Weber, T. A. Packing structures and transitions in liquids and solids. *Science* **225**, 983–989 (1984).
- Debenedetti, P. G. & Stillinger, F. H. Supercooled liquids and the glass transition. *Nature* **410**, 259–267 (2001).
- Hunter, G. L. & Weeks, E. R. The physics of the colloidal glass transition. *Rep. Prog. Phys.* **75**, 066501 (2012).
- Saika-Voivod, I., Poole, P. H. & Sciortino, F. Fragile-to-strong transition and polyamorphism in the energy landscape of liquid silica. *Nature* **412**, 514–517 (2001).
- Mauro, N., Blodgett, M., Johnson, M., Vogt, A. & Kelton, K. A structural signature of liquid fragility. *Nat. Comm.* **5**, 4616–4623 (2014).
- Stillinger, F. H. & Weber, T. A. Inherent structure theory of liquids in the hard-sphere limit. *J. Chem. Phys.* **83**, 4767–4775 (1985).
- Sciortino, F., Kob, W. & Tartaglia, P. Inherent structure entropy of supercooled liquids. *Phys. Rev. Lett.* **83**, 3214–3217 (1999).
- Auer, S. & Frenkel, D. Suppression of crystal nucleation in polydisperse colloids due to increase of the surface free energy. *Nature* **413**, 711 (2001).
- Hwang, H. J., Riggleman, R. A. & Crocker, J. C. Understanding soft glassy materials using an energy landscape approach. *Nat. Mater.* **15**, 1031 (2016).
- Bi, D., Lopez, J., Schwarz, J. & Manning, M. L. A density-independent rigidity transition in biological tissues. *Nat. Phys.* **11**, 1074 (2015).
- Berthier, L. & Witten, T. A. Glass transition of dense fluids of hard and compressible spheres. *Phys. Rev. E* **80**, 021502 (2009).
- Shen, T., Schreck, C., Chakraborty, B., Freed, D. E. & O'Hern, C. S. Structural relaxation in dense liquids composed of anisotropic particles. *Phys. Rev. E* **86**, 041303 (2012).
- Yeomans-Reyna, L. & Medina-Noyola, M. Self-consistent generalized Langevin equation for colloid dynamics. *Phys. Rev. E* **64**, 066114 (2001).



## Acknowledgements

The authors sincerely thank Prof. Walter Kob for critical reading of the manuscript and insightful comments. This study was supported by the National Natural Science Foundation of China (Grant No. 11604031) and the Fundamental Research Funds for the Central Universities of China (Grant No. 106112015CDJZR308801). Bo Li and Kai Lou acknowledge the support by Korean Institute for Basic Science (project code IBS-R020-D1). Kai Lou in addition acknowledges the support by Shenzhen Shineway Hi-Tech Co., Ltd.

## Author contributions

Z.W. and B.L. conceived the research. B.L., X.X. and Z.W. conducted the experiments with the help of K.L, S.W. and W.W.. B.L. analysed the data. B.L. and Z.W. wrote the manuscript. Z.W. and W.W. directed the project. All authors discussed on the results.

## Additional information

**Supplementary Information** accompanies this paper at <https://doi.org/10.1038/s42005-018-0081-9>.

**Competing interests:** The authors declare no competing interests.

**Reprints and permission** information is available online at <http://npg.nature.com/reprintsandpermissions/>



**Open Access** This article is licensed under a Creative Commons Attribution 4.0 International License, which permits use, sharing, adaptation, distribution and reproduction in any medium or format, as long as you give appropriate credit to the original author(s) and the source, provide a link to the Creative Commons license, and indicate if changes were made. The images or other third party material in this article are included in the article's Creative Commons license, unless indicated otherwise in a credit line to the material. If material is not included in the article's Creative Commons license and your intended use is not permitted by statutory regulation or exceeds the permitted use, you will need to obtain permission directly from the copyright holder. To view a copy of this license, visit <http://creativecommons.org/licenses/by/4.0/>.

© The Author(s) 2018